



# Visible-light-driven photocatalytic PVDF-TiO<sub>2</sub>/CNT/BiVO<sub>4</sub> hybrid nanocomposite ultrafiltration membrane for dairy wastewater treatment

Elias Jigar Sisay<sup>a,b</sup>, Gábor Veréb<sup>b</sup>, Zsolt Pap<sup>c</sup>, Tamás Gyulavári<sup>c</sup>, Áron Ágoston<sup>d</sup>, Judit Kopniczky<sup>e</sup>, Cecilia Hodúr<sup>b</sup>, Gangasalam Arthanareeswaran<sup>f</sup>, Gokula Krishnan Sivasundari Arumugam<sup>f</sup>, Zsuzsanna László<sup>b,\*</sup>

<sup>a</sup> Doctoral School of Environmental Sciences, University of Szeged, H-6720, Rerrich Béla Sqr. 1, Hungary

<sup>b</sup> Department of Biosystems Engineering, Faculty of Engineering, University of Szeged, H-6725, Szeged, Moszkvai Blvd. 9, Hungary

<sup>c</sup> Department of Applied and Environmental Chemistry, Institute of Chemistry, University of Szeged, Rerrich Béla Sqr. 1, H-6720 Szeged, Hungary

<sup>d</sup> Department of Physical Chemistry and Materials Science, University of Szeged, Rerrich Béla Sqr. 1, H-6720, Szeged, Hungary

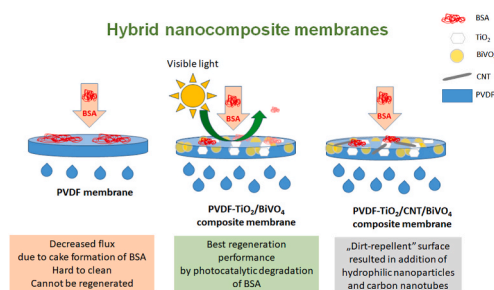
<sup>e</sup> Department of Optics and Quantum Electronics, Institute of Physics, University of Szeged, Szeged, H-6720, Dóm Sqr. 9., Hungary

<sup>f</sup> Membrane Research Laboratory, Department of Chemical Engineering, National Institute of Technology, Tiruchirappalli, 620015, India

## HIGHLIGHTS

- Photocatalytic PVDF-TiO<sub>2</sub>/CNT, PVDF-TiO<sub>2</sub>/BiVO<sub>4</sub> and PVDF-TiO<sub>2</sub>/CNT/BiVO<sub>4</sub> hybrid membranes were fabricated and characterized.
- Membranes exhibited good flux and antifouling property; PVDF-TiO<sub>2</sub>/CNT/BiVO<sub>4</sub> membranes had the best antifouling property.
- BSA rejection of PVDF-TiO<sub>2</sub>/CNT/BiVO<sub>4</sub> surpassed 97% under high water flux (150.52 L m<sup>-2</sup> h<sup>-1</sup>).
- Hybrid photocatalytic membranes showed good photocatalytic regeneration performance under visible light, PVDF-TiO<sub>2</sub>/BiVO<sub>4</sub> provided the best, 70% flux recovery ratio.

## GRAPHICAL ABSTRACT



## ARTICLE INFO

Handling Editor: Palanivel Sathishkumar

Keywords:

PVDF  
Nanocomposite membranes  
Fouling  
Visible light regeneration  
Titanium dioxide  
Bismuth vanadate  
Carbon nanotube

## ABSTRACT

Enhancing the performance of polymeric membranes by nanomaterials has become of great interest in the field of membrane technology. The present work aimed to fabricate polyvinylidene fluoride (PVDF)-hybrid nanocomposite membranes and modify them with TiO<sub>2</sub> and/or BiVO<sub>4</sub> nanoparticles and/or carbon nanotubes (CNTs) in various ratios. Their photocatalytic performance under visible light was also investigated. All modified PVDF membranes exhibited higher hydrophilicity (lower contact angle of water droplets) than that of the neat membrane used as a reference. The membranes were characterized by using bovine serum albumin (BSA) as model dairy wastewater. The hybrid membranes had better antifouling properties as they had lower irreversible filtration resistance than that of the neat membrane. Hybrid PVDF membranes containing TiO<sub>2</sub>/CNT/BiVO<sub>4</sub> showed the highest flux and lowest irreversible resistance during the filtration of the BSA solution. PVDF-TiO<sub>2</sub>/

\* Corresponding author. Department of Process Engineering, Faculty of Engineering, University of Szeged, H-6725 Szeged, Moszkvai Blvd. 9, Hungary.

E-mail addresses: [eliasjig@gmail.com](mailto:eliasjig@gmail.com) (E.J. Sisay), [verebg@mk.u-szeged.hu](mailto:verebg@mk.u-szeged.hu) (G. Veréb), [pszolt@chem.u-szeged.hu](mailto:pszolt@chem.u-szeged.hu) (Z. Pap), [gyulavarit@chem.u-szeged.hu](mailto:gyulavarit@chem.u-szeged.hu) (T. Gyulavári), [agostona@chem.u-szeged.hu](mailto:agostona@chem.u-szeged.hu) (Á. Ágoston), [jkopniczky@titani.physx.u-szeged.hu](mailto:jkopniczky@titani.physx.u-szeged.hu) (J. Kopniczky), [hodur@mk.u-szeged.hu](mailto:hodur@mk.u-szeged.hu) (C. Hodúr), [arthanaree10@yahoo.com](mailto:arthanaree10@yahoo.com) (G. Arthanareeswaran), [gokulakrishnanbio@gmail.com](mailto:gokulakrishnanbio@gmail.com) (G.K. Sivasundari Arumugam), [zsizsu@mk.u-szeged.hu](mailto:zsizsu@mk.u-szeged.hu) (Z. László).

<https://doi.org/10.1016/j.chemosphere.2022.135589>

Received 31 March 2022; Received in revised form 4 June 2022; Accepted 30 June 2022

Available online 5 July 2022

0045-6535/© 2022 The Authors. Published by Elsevier Ltd. This is an open access article under the CC BY-NC-ND license (<http://creativecommons.org/licenses/by-nc-nd/4.0/>).

BiVO<sub>4</sub> had the highest flux recovery ratio under visible light (70% for the PVDF mixed with 0.5% TiO<sub>2</sub> and 0.5% BiVO<sub>4</sub>). The hydrophilicity of membrane surfaces increased with the incorporation of nanoparticles, preventing BSA to bind to the surface. This resulted in a slight decrease in BSA and chemical oxygen demand rejections, which were still above 97% in all cases.

## 1. Introduction

Currently, membrane separation processes attract considerable attention because they have excellent contaminant rejection and low cost, and can be integrated with other processes (Gong et al., 2012; Farahani and Vatanpour, 2018; Pal, 2020; Chen et al., 2019; Li et al., 2021; Catenacci et al., 2020). In these processes, ultrafilter membranes have received widespread interest due to their capability to efficiently reject macromolecules, colloids, bacteria, and particles (Ayyaru and Ahn, 2017; Al Aani et al., 2020). Polyvinylidene fluoride (PVDF) is a polymeric material broadly applied in ultrafiltration due to its superior physical, chemical, and mechanical properties (Ji et al., 2015). However, PVDF membranes are susceptible to being fouled by wastewaters containing proteins, oils, and natural organic matter. This decreases membrane performance by lowering the flux, reducing the shelf life, and increasing the operating cost of filtration (Chang et al., 2019).

Fabricating photocatalytic membranes with excellent antifouling properties, superior flux, and better shelf life is a novel research topic in the field of membrane separation (Farahani and Vatanpour, 2018; Riaz and Park, 2019). Titanium dioxide (TiO<sub>2</sub>) is among the most widely used photocatalysts in wastewater treatment applications because it is available in large quantities, cheap, chemically stable, hydrophilic, and known mainly as a nontoxic material (Leong et al., 2014). However, it can only be efficiently activated under UV light ( $\lambda < 390$  nm for anatase) due to its relatively wide band gap of  $\sim 3.15$  eV (Akhavan, 2009). Moreover, it has two main limitations that constrain its practical application: the high recombination ratio of photocatalytically generated electron-hole pairs and the inability to utilize visible light efficiently (Zouzelka et al., 2016). To improve the photocatalytic efficiency of TiO<sub>2</sub>, structural improvements are needed (Malato et al., 2009). These can be done, for example, (i) by the combination of a photocatalyst with another semiconductor that has a narrower band gap (Malathi et al., 2018; Ratova et al., 2018); (ii) by doping with materials such as sulfur, transition metal ions, noble metals, or nitrogen (Malato et al., 2009); or (iii) by applying a suitable photosensitizer (Yogarathinam et al., 2018). In recent years, bismuth-based oxides have received considerable attention and been reported as efficient visible-light-active photocatalysts. This is because of their narrow band gap that enables the absorption of visible light, however, their relatively low surface area and activity limits their application.

Carbon nanotubes (CNTs) are semiconductor materials, which are broadly used as electron acceptors and may notably hinder the recombination of photogenerated electron-hole pairs in TiO<sub>2</sub> (Selvaraj et al., 2020). Besides, in recent articles on functionalised CNT and PVDF composite membranes (CNT/PVDF) better water fluxes, excellent protein removal and improved hydrophilic characters have been reported (Moslehyani et al., 2015; Ayyaru et al., 2019).

Due to the beneficial properties of the materials described above, their combination may result in a novel PVDF-TiO<sub>2</sub>/CNT/BiVO<sub>4</sub> nanocomposite membrane of superior characteristics. They may not only have better antifouling performance but also the possibility to be regenerated under visible light irradiation. In this study, we aimed to develop visible-light-active PVDF-TiO<sub>2</sub>/CNT/BiVO<sub>4</sub> photocatalytic composite membranes and evaluate their applicability for the treatment of a model dairy wastewater. As the main fouling components of dairy wastewaters are proteins, in our examinations bovine serum albumin (BSA) solution was used as model dairy wastewater.

## 2. Experimental design

### 2.1. Materials

Analytical grade PVDF powder, N-methyl-2-pyrrolidone (NMP) solvent, and sodium dodecyl sulfate surfactant were bought from Merck Hungary and used for membrane preparation. BSA (69 kDa) was purchased from ICN Biomedicals Inc. (USA). The commercial nanoparticles used were Aeroxide P25 TiO<sub>2</sub> (Merck EMD Millipore Co., Germany) and multiwalled CNTs (Kanto Chemical Co. Inc.; TNMH3 15090, Japan; >98 wt%). Bismuth(III) nitrate pentahydrate (Alfa Aesar,  $\geq 98\%$ , ACS), ammonium vanadate (Sigma Aldrich,  $\geq 98\%$ ), sodium hydroxide (Sigma-Aldrich, 100%, puriss), and nitric acid (Merck, 99%) were used to synthesize bismuth vanadate (BiVO<sub>4</sub>).

### 2.2. Methods

The BiVO<sub>4</sub> nanoparticles were synthesized via a hydrothermal method as described earlier in the work of Nascimben et al. (2020), in which they were referred to as the BiVO<sub>4</sub>-I sample. The band gap of this sample was calculated to be 2.35 eV.

The methods of investigation of photocatalytic activity of the nanoparticles were presented in the [Supplementary Material Section S1](#).

#### 2.2.1. Membrane preparation

Neat and modified ultrafilter PVDF membranes were prepared via a non-solvent-induced phase-inversion method according to the publication of Harsha et al., (2011). The composition of casting dope solutions and the names of the membranes are given in [Table 1](#). First, the PVDF powders and nanoparticles (TiO<sub>2</sub> and/or BiVO<sub>4</sub> and/or CNT) were kept in an oven at 80 °C for 4 h. Then, the nanoparticles were suspended in 20 mL of NMP and ultrasonicated for 60 s. Second, the dried PVDF powder was mixed with the suspension and kept at 50 °C in the dark for 12 h for both steps. Third, the possible air bubbles of the casting dope solution were removed by ultrasonication for 30 min. Then, the solution was poured onto a glass plate and casted with a casting blade at 400  $\mu$ m thickness. The layer casted on the plate was kept at rest for 30 s to enable the formation of a skin layer. After that, the layer was put into a bath solution containing sodium dodecyl sulfate surfactant in 3 g L<sup>-1</sup>. The

**Table 1**  
Composition and names of the membranes.

Membrane	17.5 wt% PVDF or 16.5 wt% PVDF +1 wt% nanoparticles				82.5 wt% (Solvent)
	PVDF (g)	TiO <sub>2</sub> (mg)	CNT (mg)	BiVO <sub>4</sub> (mg)	NMP (mL)
PVDF	4.375	–	–	–	20
PT100	4.331	43.750	–	–	20
PTC2	4.331	42.875	0.875	–	20
PTC5	4.331	41.560	2.190	–	20
PTC10	4.331	39.375	4.375	–	20
PTC15	4.331	37.188	6.5625	–	20
PTB25	4.331	32.813	–	10.938	20
PTB50	4.331	21.875	–	21.875	20
PTB75	4.331	10.938	–	32.813	20
PB100	4.331	–	–	43.750	20
PTCB25	4.331	31.938	0.875	10.938	20
PTCB50	4.331	21.000	0.875	21.875	20
PTCB75	4.331	10.061	0.875	32.813	20

system was kept at 10 °C for 3 h before storing it in distilled water overnight. Phase inversion took place in the coagulation bath between the water and NMP, resulting in the formation of pores. The surfactant was used to clean the pores and prevent pore blockage. Last, the membranes were cut to the required size for the ultrafiltration experiments.

### 2.2.2. Membrane filtration experiments

Filtration performance experiments were carried out using 1 g L<sup>-1</sup> BSA solution as a model dairy wastewater (Ding et al., 2018) since this concentration represents a realistic protein content for dairy wastewater. The surface area of the membrane was 0.0035 m<sup>2</sup> and the filtration experiments were conducted using a dead-end filtration cell (Millipore, XFUF04701, USA). Before carrying them out, ultrapure water was filtered through the given membrane for 30 min (0.1 MPa transmembrane pressure) for compaction, to achieve a constant water flux. In each experiment, the feed solution was let to pass through the membrane until the volume reduction ratio (VRR) reached five. The applied transmembrane pressure was 0.1 MPa and the filtration cell was stirred at 350 rpm.

Flux recovery experiments were performed in the same reactor. After the filtration of BSA, the membranes were carefully flushed, and the water fluxes were measured. The fluxes were remeasured after 3 and 21 h of UV (Lightech, λ = 360 nm, 10 W; for TiO<sub>2</sub> and/or CNT-containing composites) or visible light (Lightech Vis, 10 W, for BiVO<sub>4</sub>-containing composites) irradiation to evaluate the efficiency of photocatalytic flux recovery.

### 2.2.3. Characterization of membranes

The porosity of membranes was determined by measuring the weight of the wet and dry membranes (Srivastava et al., 2011). First, the surface of the wet membrane was wiped to remove the water from the surface, then, the wet weight was measured immediately. Second, the wet membrane was dried for 12 h at 80 °C in a vacuum oven before measuring its dry weight. The porosity was obtained using Eqs. (1) and (2):

$$\text{Porosity} = \frac{W_1 - W_2}{\rho_w \times VT} \cdot 100 \quad (1)$$

$$VT = \frac{W_1 - W_2}{\rho_w} + \frac{W_2}{\rho_{md}} \quad (2)$$

where  $W_1$  and  $W_2$  are the wet and dry weights, respectively,  $VT$  is the volume of the wet membrane (m<sup>3</sup>),  $\rho_w$  is the density of water (997 kg m<sup>-3</sup>), and  $\rho_{md}$  is the density of the dry membrane (1785 kg m<sup>-3</sup>).

The membranes' pore sizes were obtained by calculating the mean pore radius ( $r_m$ ) using Eq. (3) (Ayyaru et al., 2019):

$$r_m = \sqrt{\frac{(2.9 - 1.75 \epsilon) \cdot 8\eta l Q}{\epsilon \cdot A \cdot P}} \quad (3)$$

where  $\epsilon$  is porosity (calculated by the method described above),  $A$  is the area of the membrane (m<sup>2</sup>);  $P$  is the transmembrane pressure (applied during the filtration of clean water),  $\eta$  is the viscosity of the used water (8.9·10<sup>-4</sup> Pa s);  $Q$  is the measured water flux (m<sup>3</sup>·s<sup>-1</sup>), and  $l$  is the thickness of the membrane (400 μm).

Specific surface area measurements were performed for three modified membranes (neat PVDF, PT100 and PB100) by recording nitrogen adsorption-desorption isotherms on a Quantachrome Nova 3000e instrument at -196 °C. The apparent surface areas ( $S_{BET}$ ) were calculated via the Brunauer-Emmett-Teller (BET) model. The total pore volumes ( $V$ ) were derived from the amount of nitrogen adsorbed at different relative pressures ( $p/p_0$ ) presuming that the pores were filled with liquid nitrogen. The pore size distribution was calculated from the desorption branch of the isotherms using the Barrett-Joyner-Halenda (BJH) method. The average pore diameter was estimated by using Eq. (4):

$$d = \frac{4V}{A} \quad (4)$$

For the description of the hydrophilicity of neat and modified membranes, contact angle measurements were carried out by using the sessile-drop method with an OCA15Pro contact angle meter (Data-Physics, Germany). It was adjusted to drop 10 μL of ultrapure water onto the surface of membranes with a microsyringe. Subsequently, the image of the water droplet was taken with a digital camera, and the software (ImageJ) was used for image processing. Six parallel measurements were carried out.

The morphology of the membranes' surface was analyzed with a Hitachi S-4700 Type II scanning electron microscope (SEM) using 10 kV accelerating voltage. The elemental analysis of the fouled membrane was carried out with a Röntec X-Flash energy dispersive X-ray (EDX) detector (20 keV). The N/F ratio of the samples was calculated based on their N and F contents (calculated in both at% and wt% by the instrument) to reveal the coverage of BSA on the membranes. For these measurements, 200 mL of BSA solution (1 g L<sup>-1</sup>) was filtered through the membrane, which was then dried and used without washing.

X-ray diffraction (XRD) measurements were performed to determine the primary crystallite size of the nanoparticles in the membranes using a Rigaku MiniFlex II diffractometer. For this purpose, the equipment was operated at 30 kV and 15 mA using Cu-K<sub>α</sub> radiation (λ = 0.015406 nm), and the XRD patterns were recorded between 20 and 40° (2θ°). The primary crystallite sizes were calculated based on the Scherrer equation (HolzwarthGibson, 2011).

The surface roughness was measured with a PSIA XE-100 atomic force microscope (AFM; South Korea; NC-AFM head mode, 10 × 10 μm scan size) by evaluating the Rq values.

Fluxes were calculated by Eq. (5) as follows:

$$J = \frac{W}{A \cdot t} \quad (5)$$

where  $J$  is the flux (kg·m<sup>-2</sup>·h<sup>-1</sup>),  $W$  is the weight of permeate (kg),  $A$  is the effective surface area of the membrane (m<sup>2</sup>), and  $t$  is the time required to complete filtration (h).

The VRR was obtained by Eq. (6):

$$\text{VRR} = \frac{V_0}{V_0 - V_f} \quad (6)$$

where  $V_0$  and  $V_f$  are the initial and final volumes, respectively.

The rejection of protein was obtained by Eq. (7):

$$\text{Rejection}(\%) = \frac{c_1 - c_2}{c_1} \times 100\% \quad (7)$$

where  $c_1$  and  $c_2$  are the concentrations of contaminants before and after filtration, respectively.

Membrane fouling was followed by calculating the filtration resistances using the resistance-in-series model. The total filtration resistance (Eq. (8)) was given as the sum of membrane resistance ( $R_M$ ) and reversible ( $R_r$ ) and irreversible ( $R_{ir}$ ) resistances. These were calculated from the fluxes measured in clean membranes, fluxes after the filtration of BSA, and after rinsing the used membrane (Nascimben et al., 2020):

$$R_T = R_M + R_r + R_{ir} \quad (8)$$

Antifouling performance of the membranes (Eq. (9)) was evaluated based on the same experiment used for the calculation of flux recovery ratio (FRR):

$$\text{FRR} = \frac{J_c}{J_0} \cdot 100 \quad (9)$$

where  $J_0$  is the flux of pure water (L·m<sup>-2</sup>·h<sup>-1</sup>) before filtrating the BSA solution, and  $J_c$  is the flux of pure water after rinsing the used membrane (L·m<sup>-2</sup>·h<sup>-1</sup>).

Water permeability of the membranes were modeled by Hermia fouling models as presented in Supplementary Material S3. section.

The concentration of BSA in the model dairy wastewater was measured before and after filtration by a spectrophotometric method. The measurement was based on recording the absorbance of BSA at a wavelength of 280 nm using a UV–visible spectrophotometer (Hitachi Co., U-2000, Japan). The concentration values were obtained from a calibration curve (Yan et al., 2021).

COD of the samples was determined via the potassium–dichromate oxidation method. The samples (2 mL) were added to test tubes (Merck; in concentrations of 0–150 or 0–1500 mg L<sup>-1</sup>) and digested for 2 h at 150 °C (Lovibond, ET 108). Then, the absorbances were measured with a spectrophotometer (Lovibond PC-CheckIt).

### 3. Results and discussion

#### 3.1. Characterization of membranes

The crystalline structure of the samples was investigated by XRD measurements and patterns characteristic of TiO<sub>2</sub>, BiVO<sub>4</sub>, and multi-walled CNTs were expected to appear. It should be noted that their concentration was low, hence the calculations possess a 15% error margin (Fig. S2). The XRD patterns of the base PVDF membrane showed a major diffraction peak below 22° and some weaker signals at 25.28, 26.98, 31.62, and 36.02°. The first signal was removed to enhance the interpretability and readability of the figure. For CNTs the (002) crystallographic plane, which is the most intense one, can be located at 25.8° (JCPDS card. No. 96-101-1061). However, it overlapped with the other investigated compounds, hence no relevant information was found for CNTs. Diffraction peaks characteristic of monoclinic BiVO<sub>4</sub> (JCPDS No. 14–0688) were identified in PTBC50, PTB50, and PB100 with a primary crystallite size of 16.4 nm. The (101) plane of anatase TiO<sub>2</sub> was clearly identifiable via the major diffraction peak at 25.38° (JCPDS No. 21–1272). The calculated primary crystallite size was 20.4 nm (in accordance with that of Evonik Aeroxide P25 for anatase). In PTBC50 and PTB50 the signals of TiO<sub>2</sub> were particularly weak but visible via the signal at 25.38°.

For the determination of average pore sizes, two different methods were used. However, it is important to highlight that both methods have limitations. First, the calculations were based on flux measurements (Eqs. (1)–(3)), which are dependent not only on the pore size, but on the wettability of the membrane too. In order to reveal these effects, BET measurements were performed and the specific surface area and pore size distribution of the neat PVDF, PT100 and PB100 membranes were determined (Fig. 1).

Based on the pore size distribution curves, many small pores could be observed, which probably did not have a role in filtration. However, their presence resulted in a lower average pore size than that obtained

from other measurements. These results show that the presence of nanoparticles in PVDF had only a limited effect on the pore size distribution.

The pore size and porosity values determined by Eqs. (1)–(3) and the wettability data are presented in Table 2. Higher porosities were calculated for the modified membranes (84.71–89.50%) compared to the pristine one (84.0%). PTCB50 showed the highest porosity with a value of 89.50%. The porosity and pore size results we obtained were close to the ones obtained by Hudaib et al., 2018. and Farahani and Vatanpour., 2018.

The wettability of the membranes was determined by contact angle measurements (Table 2). The average contact angle value was 78.10 ± 5.99° for the pristine PVDF membrane. The wettability of all modified membranes was smaller than this value. This implies that the incorporated TiO<sub>2</sub> or BiVO<sub>4</sub> nanoparticles increased the hydrophilicity of the PVDF membrane and resulted in higher water permeability. The contact angle of the membranes was also decreasing with the increasing concentration of CNTs in TiO<sub>2</sub>/CNT, which resulted in an increased flux. Our results are in good accordance with the results of Yi et al. (2016). They showed that TiO<sub>2</sub>/CNT composites have higher hydrophilicity even than TiO<sub>2</sub>. Moreover, in CNT-containing composite membranes the open ends of CNTs, which are hydrophobic, might create strong bonds with the fluoride ions in PVDF resulting in highly hydrophilic membranes (Wang et al., 2015; Dhand et al., 2019). The contact angles of all BiVO<sub>4</sub>-modified membranes were also lower than that of the pristine membrane. This was expected due to the hydrophilic nature of pure BiVO<sub>4</sub> (Pi et al., 2021), similarly to the results of TiO<sub>2</sub>-modified membranes.

The water fluxes of the membranes are shown in Table 2. All nanocomposite membranes exhibited higher flux than that of the pristine PVDF membrane. The best results were obtained for the BiVO<sub>4</sub>-containing membranes. Although the water flux of PVDF-TiO<sub>2</sub>/CNT increased with increasing CNT content, the addition CNTs in 2% slightly decreased water fluxes for both TiO<sub>2</sub> and BiVO<sub>4</sub> composites.

Five membranes (PVDF, PT100, PB100, PTB50 and PTBC50) were selected to study their morphology. AFM measurements revealed (Fig. 2a and Table 3) that the nanocomposite membranes had slightly rougher surfaces than that of the neat PVDF membrane. This can be explained by the presence of aggregated (200–300 nm) nanoparticles on the surface. Although the primary crystallite sizes were in the range of 10–25 nm (according to XRD results), SEM micrographs revealed that both TiO<sub>2</sub> and BiVO<sub>4</sub> particles were present as aggregates in the membrane material (Table 3).

The pristine PVDF membrane showed a good rejection for BSA (99.79 ± 0.09%) and BSA expressed in COD (99.75 ± 0.08) (Table 2). The rejection performances of modified membranes were slightly lower than that of the pristine PVDF membrane; however, they were still above 97% for BSA and 96% for COD. The lower rejection values may be explained by the change in the distribution of BSA on the surface (Fig. 2b and Table 3). The proteins may have covered a relatively large area of the neat PVDF membrane, resulting in a relatively high N/F ratio (Fig. 2b.) obtained from EDX measurements. As a “protein layer” is developed on the surface of the membrane, it acts as an additional filter, “trapping” most of the BSA molecules. In composite membranes, the BSA formed smaller and more compact particles, leaving more uncovered areas on the surface. This is supported by the decreased N/F ratio too. Without the “protein layer”, more BSA molecules can get across the membrane, resulting in decreased rejection. Although there is an inverse correlation between surface roughness and protein coverage, the shape of BSA molecules on the surface makes the following explanation plausible: the addition of nanoparticles changes surface charge, which affects the binding of BSA to the surface, rather than the morphology of the surface.

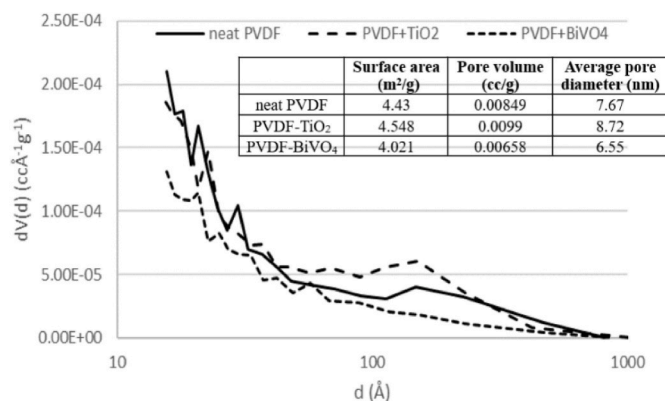
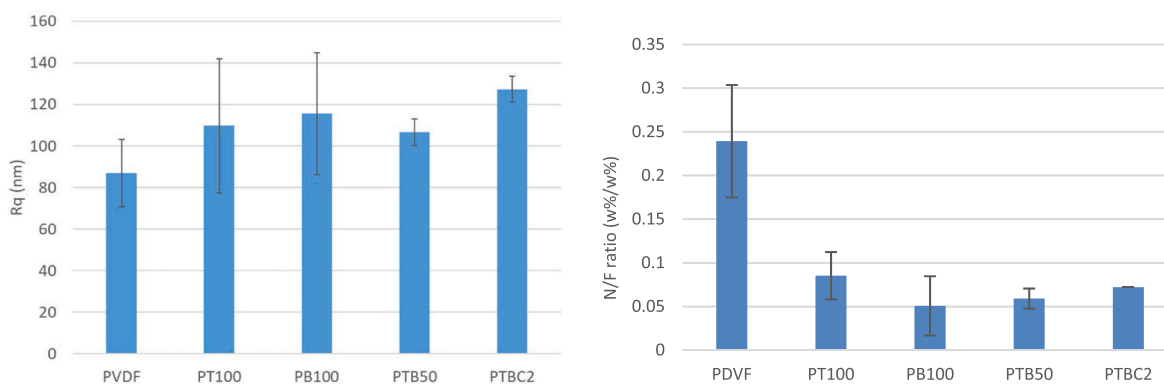


Fig. 1. Pore size distributions of neat and composite membranes determined by the BJH approach from the BET adsorption–desorption isotherms.

**Table 2**  
Characteristics of neat PVDF membrane and membranes modified with TiO<sub>2</sub> and BiVO<sub>4</sub> and CNTs.

Membrane type	Porosity (%)	Mean pore size (nm)	Contact angle (°)	Water flux (L·m <sup>-2</sup> ·h <sup>-1</sup> )	Rejection (%)	
					BSA	COD
PVDF	84.00 ± 0.00	30.04 ± 0.04	78.10 ± 5.99	67.22 ± 0.7	99.79 ± 0.09	99.75 ± 0.08
PT100	85.30 ± 0.02	33.43 ± 0.58	73.45 ± 4.30	85.63 ± 0.66	98.87 ± 0.60	99.74 ± 0.09
PTC2	85.43 ± 0.06	33.52 ± 0.21	71 ± 5.3	82.23 ± 0.09	98.89 ± 0.10	99.34 ± 0.12
PTC5	85.73 ± 0.03	32.81 ± 0.19	67.45 ± 3.50	81.07 ± 0.05	97.45 ± 0.34	97.05 ± 0.34
PTC10	84.93 ± 0.01	36.31 ± 0.24	66.05 ± 7.00	92.26 ± 0.08	98.55 ± 0.25	98.13 ± 0.6
PTC15	86.82 ± 0.07	40.78 ± 0.17	65.67 ± 5.00	110.78 ± 0.07	98.79 ± 0.28	96.98 ± 0.2
PTB25	86.54 ± 0.00	40.85 ± 2.97	69.68 ± 3.24	131.79 ± 2.07	97.09 ± 0.16	96.88 ± 0.09
PTB50	85.59 ± 0.00	44.61 ± 8.00	62.3 ± 4.24	153.56 ± 1	97.75 ± 0.03	97.48 ± 0.15
PTB75	84.80 ± 0.00	34.87 ± 0.00	71.35 ± 2.73	92.06 ± 1.2	98.01 ± 0.09	94.96 ± 0.02
PB100	83.38 ± 0.00	47.33 ± 0.11	76.53 ± 2.42	163.87 ± 3.23	98.01 ± 0.0	96.68 ± 0.75
PTCB25	85.35 ± 0.00	43.00 ± 0.03	72.74 ± 2.58	141.78 ± 2.51	98.88 ± 1.0	98.31 ± 0.25
PTCB50	89.50 ± 0.00	34.50 ± 0.00	69.875 ± 5.01	150.52 ± 2.04	97.10 ± 0.77	95.51 ± 0.15
PTCB75	84.71 ± 0.00	26.12 ± 0.00	69.53 ± 2.39	86.27 ± 1.09	97.75 ± 0.09	96.72 ± 0.11



**Fig. 2.** (a) Surface roughness of neat PVDF and composite membranes; (b) N/F ratio in the fouled membrane.

### 3.2. Fouling mitigation and regeneration of nanocomposite membranes

The filtration resistances of the membranes, caused by the filtration of BSA solutions, were described by calculating their total resistances ( $R_T$ ), membrane resistances ( $R_M$ ), irreversible resistances ( $R_{ir}$ ), and reversible resistances ( $R_r$ ). The results are summarized in Fig. 3a–c. The highest total resistance was observed for the pristine PVDF membrane, and in comparison, all modified membranes were more beneficial in terms of irreversible fouling. This may be explained by the lower surface charge of the modified membranes as it was observed for TiO<sub>2</sub>-modified PVDF membranes also by Man et al. (2020). Negatively charged surfaces leads to the repulsion of negatively charged BSA, preventing protein fouling. Moreover, the water flux exhibited an increasing trend with increasing CNT concentration in case of PTC2-PTC15 membranes (Table 2, Fig. 3a), which can be explained by the increased hydrophilicity confirmed by contact angle measurements. The lowest total resistance was achieved for PTC2, that is, the TiO<sub>2</sub>/CNT composite membrane with 2% CNT content. This means that this CNT concentration had to be used to achieve the best fluxes and the lowest irreversible resistance during the filtration of BSA. Increasing CNT loading increased fouling, which probably can be explained by the hydrophobic nature of CNTs that may adsorb the hydrophobic parts of protein molecules.

In the next series of experiments the effect of BiVO<sub>4</sub> addition on fouling mitigation was examined. The addition of BiVO<sub>4</sub> nanoparticles considerably reduced filtration resistance (Fig. 3b) and had a slightly more beneficial effect than TiO<sub>2</sub> addition. Fig. 3c shows the filtration PVDF-TiO<sub>2</sub>/CNT/BiVO<sub>4</sub> composites with different BiVO<sub>4</sub> and 2% CNT content. Similarly to the previous experiments, the addition of CNTs in 2% resulted in the best performance. BiVO<sub>4</sub> addition decreased total filtration resistance during the filtration of BSA (except for PTCB75), but irreversible resistances slightly increased in the presence of BiVO<sub>4</sub>.

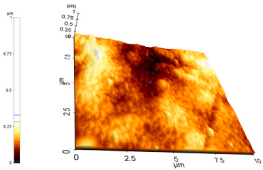
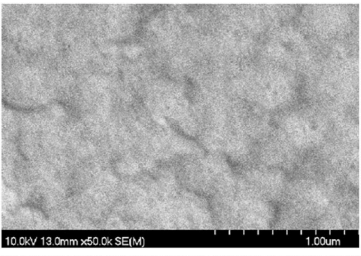
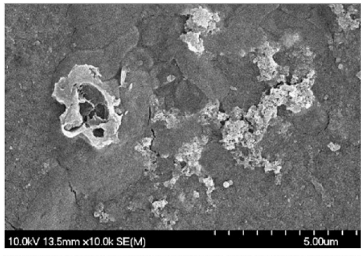
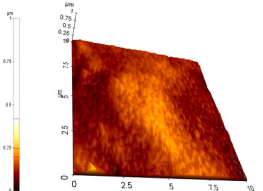
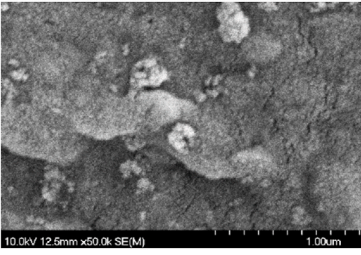
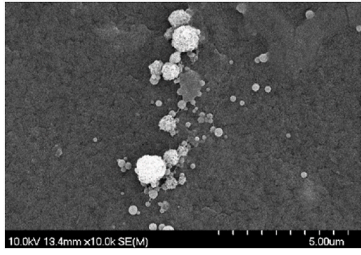
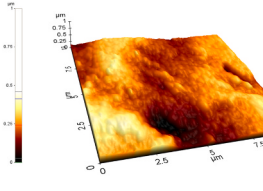
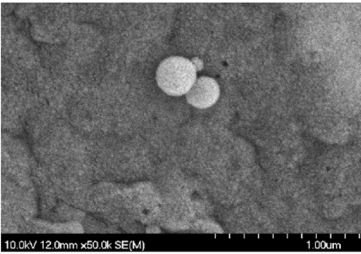
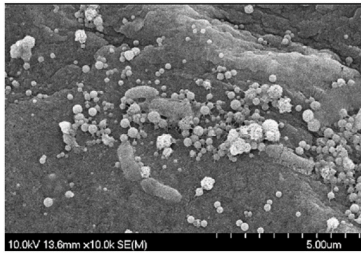
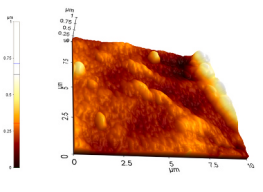
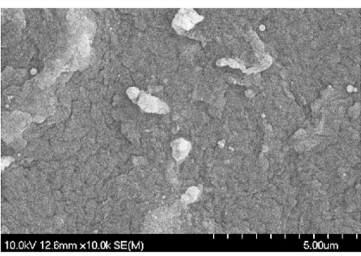
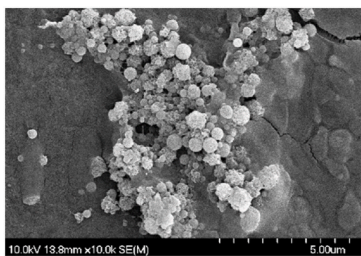
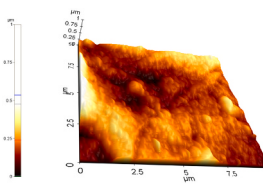
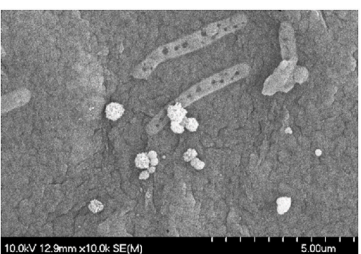

FRR values of nanocomposite membranes are very informative to evaluate their cleanability. Thus, these values were calculated and the results are presented in Fig. 3d–f. For the regeneration of TiO<sub>2</sub>/CNT composites, UV light was used as TiO<sub>2</sub> can only be excited efficiently by it. Water flux increased with increasing CNT concentration, but the fouling pattern was different, as the irreversible fouling was more extended. This phenomenon was also observed in the cleanability of the membranes. Membranes with higher CNT content were less cleanable by UV radiation; PT100 and PTC2 provided the highest FRR (Fig. 3d).

BSA-fouled BiVO<sub>4</sub>-containing membrane surfaces were regenerated by using visible-light-induced photocatalytic purification (Fig. 3e). The restoration of flux for all BiVO<sub>4</sub>-based membranes was more efficient than that for the pristine PVDF membrane, even without utilizing the photocatalytic effect of BiVO<sub>4</sub>. In the case of photocatalytic regeneration, it was revealed that the mixed PVDF-TiO<sub>2</sub>/BiVO<sub>4</sub> composites had better performance than that of PVDF-BiVO<sub>4</sub>. The regeneration performance increased with increasing BiVO<sub>4</sub> concentration, as was expected due to its photocatalytic activity under visible light. However, the presence of TiO<sub>2</sub> is necessary to reach superior performance. Regeneration of BSA-fouled PVDF-TiO<sub>2</sub>/CNT/BiVO<sub>4</sub> membrane surfaces with visible-light-induced photocatalytic purification is demonstrated in Fig. 3f. The restoration of flux for CNT/BiVO<sub>4</sub>-containing membranes was better than that for BiVO<sub>4</sub>-containing membranes without photocatalysis. However, the presence of CNTs decreased the efficiency of photocatalytic regeneration, probably due to the light absorption of CNTs.

## 4. Conclusions

This work aimed to produce hybrid nanocomposite PVDF membranes by the addition of TiO<sub>2</sub>, and/or CNT, and/or BiVO<sub>4</sub>, and to

**Table 3**  
AFM and SEM micrographs of the surface of the membranes.

Mem-brane	AFM micrographs	SEM micrographs of the top of the membranes	SEM micrographs of BSA-fouled membranes
PVDF			
PT100			
PB100			
PTB50			
PTBC50			

investigate their antifouling performance during the filtration of a model dairy wastewater (BSA solution). Another goal of this study was to examine the regeneration performance of the fouled membranes under UV or visible light.

PVDF-TiO<sub>2</sub>/CNT/BiVO<sub>4</sub> membranes were fabricated by a phase inversion method. XRD and SEM measurements revealed that the nanoparticles were present as 200–300 nm-sized aggregates in the membrane, which increased the roughness of composite membranes. Nevertheless, the hybrid membranes showed excellent antifouling properties, higher flux, and lower filtration resistance than those of the pristine membrane. It was deduced that the protein molecules could not “expand” on the surface; thus, they covered only a relatively small area of the composite membranes compared to the neat PVDF membrane. The addition of TiO<sub>2</sub> resulted in better performance than that of the neat membrane. This could be further enhanced by the addition of CNTs,

which resulted in enhanced hydrophilicity and filtration performance. The best results were obtained by adding CNT in 2% since higher concentrations increased irreversible fouling. The addition of both BiVO<sub>4</sub> and TiO<sub>2</sub> resulted in composite membranes with better performance than that of composite membranes containing only TiO<sub>2</sub> or BiVO<sub>4</sub>. The best antifouling performances were obtained for the PVDF-TiO<sub>2</sub>/CNT/BiVO<sub>4</sub> composites. The best sample was the one where the ratio of nanoparticles used was 2 wt% CNT and 50–50 wt% TiO<sub>2</sub> and BiVO<sub>4</sub> respectively. However, the best performance in terms of regeneration under visible light was achieved for the PVDF-TiO<sub>2</sub>/BiVO<sub>4</sub> composites. Composite membranes exhibited comparable, but slightly lower BSA and COD rejections than those of the pristine membrane.

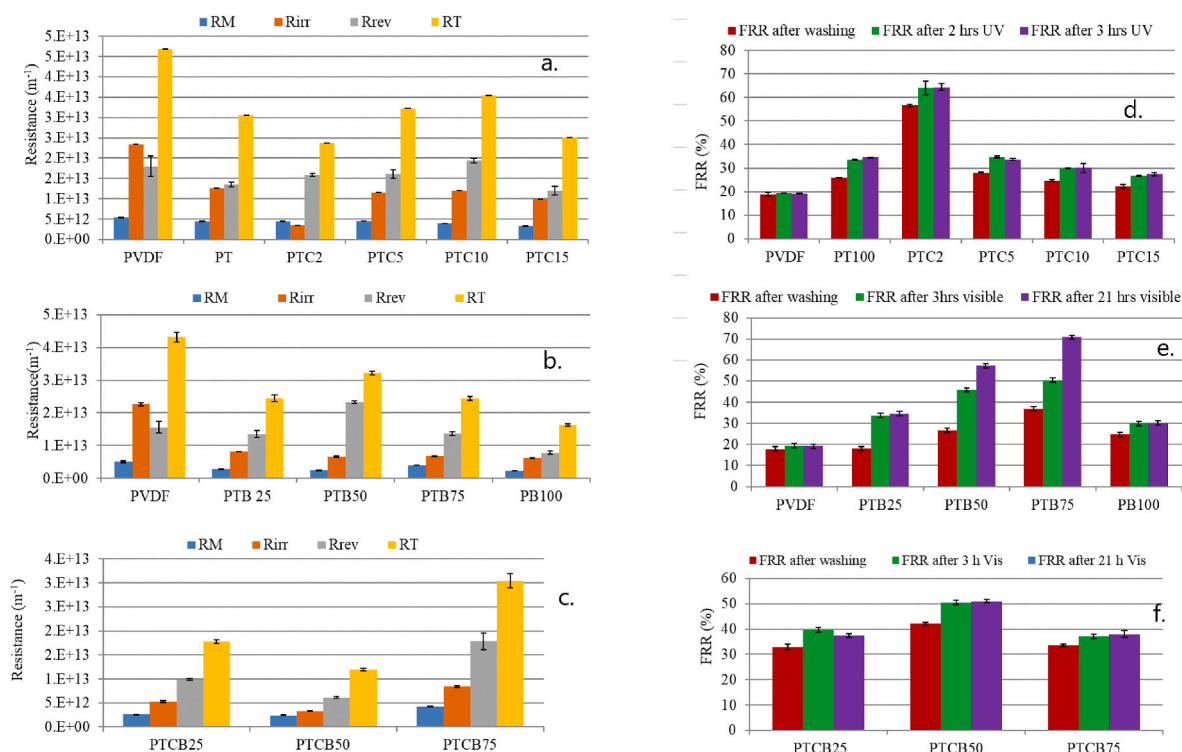


Fig. 3. Filtration resistances of (a) PVDF, PVDF-TiO<sub>2</sub>, and PVDF-TiO<sub>2</sub>/CNT-membranes, (b) PVDF, PVDF-TiO<sub>2</sub> and PVDF-TiO<sub>2</sub>/BiVO<sub>4</sub> membranes, and (c) different PVDF-TiO<sub>2</sub>/CNT/BiVO<sub>4</sub> membranes with 2% CNT content. FRRs of BSA-fouled (d) PVDF, PVDF-TiO<sub>2</sub> and PVDF-TiO<sub>2</sub>/CNT membranes, (e) PVDF, PVDF-TiO<sub>2</sub> and PVDF-TiO<sub>2</sub>/BiVO<sub>4</sub> membranes, and (f) different PVDF-TiO<sub>2</sub>/CNT/BiVO<sub>4</sub> membranes with 2% CNT content.

#### Author contribution

Conceptualization; Zsuzsanna László; , Elias Jigar Sisay Data curation; Elias Jigar Sisay, Funding acquisition; Arthanareeswaran Gangasalam, Zsuzsanna László; , Gábor Veréb, Investigation; Elias Jigar Sisay, Áron Ágoston, Gokula Krishnan, Judit Kopniczky, Methodology; Gábor Veréb, Tamás Gyulavári, Arthanareeswaran Gangasalam, Supervision; Cecilia Hodúr, Arthanareeswaran Gangasalam, Roles/Writing – original draft: Elias Jigar Writing – review & editing: Gábor Veréb, Zsuzsanna László; , Tamás Gyulavári, Zsolt Pap<a name = "Line\_credittaxonomy\_1">

#### Declaration of competing interest

The authors declare that they have no known competing financial interests or personal relationships that could have appeared to influence the work reported in this paper.

#### Data availability

Data will be made available on request.

#### Acknowledgements

The authors are grateful for the financial provision of Hungarian Science and Research Foundation, 2017–2.3.7-TÉT-IN–2017-00016 and Ministry of Science and Technology of the Government of India, DST/INT/HUN/P17/2017. The authors are also thankful for the financial support of the University of Szeged (4541) and University of Szeged Open Access Fund, Grant number 5813. Finally, Elias Jigar Sisay is thankful to Stipendium Hungaricum Scholarship for the financial support of the research.

#### Appendix A. Supplementary data

Supplementary data to this article can be found online at <https://doi.org/10.1016/j.chemosphere.2022.135589>.

#### References

- Akhavan, O., 2009. Lasting antibacterial activities of Ag-TiO<sub>2</sub>/Ag/a-TiO<sub>2</sub>nanocomposite thin film photocatalysts under solar light irradiation. *J. Colloid Interface Sci.* 336 (1), 117–124. <https://doi.org/10.1016/j.jcis.2009.03.018>.
- Al Aani, S., Mustafa, T.N., Hilal, N., 2020. Ultrafiltration membranes for wastewater and water process engineering: a comprehensive statistical review over the past decade. *J. Water Proc. Eng.* 35, 101241 <https://doi.org/10.1016/j.jwpe.2020.101241>.
- Ayyaru, S., Ahn, Y.H., 2017. Application of sulfonic acid group functionalized graphene oxide to improve hydrophilicity, permeability, and antifouling of PVDF nanocomposite ultrafiltration membranes. *J. Membr. Sci.* 525, 210–219. <https://doi.org/10.1016/j.memsci.2016.10.048>.
- Ayyaru, S., Pandiyan, R., Ahn, Y.-H., 2019. Fabrication and characterization of anti-fouling and non-toxic polyvinylidene fluoride-Sulphonated carbon nanotube ultrafiltration membranes for membrane bioreactors applications. *Chem. Eng. Res. Des.* 142, 176–188. <https://doi.org/10.1016/j.chemd.2018.12.008>.
- Catenacci, A., Bellucci, M., Yuan, T., Malpei, F., 2020. Dairy wastewater treatment using composite membranes. *Current Trends Future Dev. (Bio-) Membranes* 261–288. <https://doi.org/10.1016/b978-0-12-816823-3.00009-5>.
- Chang, Y.R., Lee, Y.J., Lee, D.J., 2019. Membrane fouling during water or wastewater treatments: current research updated. *J. Taiwan Inst. Chem. Eng.* 94, 88–96. <https://doi.org/10.1016/j.jtice.2017.12.019>.
- Chen, G.Q., Leong, T.S.H., Kentish, S.E., Ashokkumar, M., Martin, G.J.O., 2019. Membrane separations in the dairy industry. *Separat. Funct. Mol. Food Membr. Technol.* 267–304. <https://doi.org/10.1016/b978-0-12-815056-6.00008-5>.
- Dhand, V., Hong, S.K., Li, L., Kim, J.-M., Kim, S.H., Rhee, K.Y., Lee, H.W., 2019. Fabrication of robust, ultrathin and light weight, hydrophilic, PVDF-CNT membrane composite for salt rejection. *Compos. B Eng.* 160, 632–643. <https://doi.org/10.1016/j.compositesb.2018.12>.
- Ding, Y., Ma, B., Liu, H., Qu, J., 2018. Effects of protein properties on ultrafiltration membrane fouling performance in water treatment. *J. Environ. Sci.* <https://doi.org/10.1016/j.jes.2018.08.005>.
- Farahani, M.H.D.A., Vatanpour, V., 2018. A comprehensive study on the performance and antifouling enhancement of the PVDF mixed matrix membranes by embedding different nanoparticles: clay, functionalized carbon nanotube, SiO<sub>2</sub> and TiO<sub>2</sub>. *Separ. Purif. Technol.* 197, 372–381. <https://doi.org/10.1016/j.seppur.2018.01.031>.

- Gong, Y.W., Zhang, H.X., Cheng, X.N., 2012. Treatment of dairy wastewater by two-stage membrane operation with ultrafiltration and nanofiltration. *Water Sci. Technol.* 65 (5), 915–919. <https://doi.org/10.2166/wst.2012.937>.
- Holzwarth, U., Gibson, N., 2011. The Scherrer equation versus the 'Debye-Scherrer equation'. *Nat. Nanotechnol.* 6 <https://doi.org/10.1038/nnano.2011.145>, 534–534.
- Hudaib, Banan, Gomes, Vincent, Shi, Jeffrey, Zhou, Cuifeng, Liu, Zongwen, 2018. Poly(vinylidene fluoride)/Polyaniline/MWCNT nanocomposite ultrafiltration membrane for natural organic matter removal. *Separ. Purif. Technol.* 190, 143–155. <https://doi.org/10.1016/j.seppur.2017.08.026>.
- Ji, J., Liu, F., Hashim, N.A., Abed, M.R.M., Li, K., 2015. Poly(vinylidene fluoride) (PVDF) membranes for fluid separation. *React. Funct. Polym.* 86, 134–153. <https://doi.org/10.1016/j.reactfunctpolym.2014.09.023>.
- Leong, S., Razmjou, A., Wang, K., Hapgood, K., Zhang, X., Wang, H., 2014. TiO<sub>2</sub> based photocatalytic membranes. *Review* 472, 167–184. <https://doi.org/10.1016/j.memsci.2014.08.016>.
- Li, X., Shen, S., Xu, Y., Guo, T., Dai, H., Lu, X., 2021. Application of membrane separation processes in phosphorus recovery: a review. *Sci. Total Environ.* 767, 144346 <https://doi.org/10.1016/j.scitotenv.2020.144346>.
- Malathi, A., Arunachalam, P., Kirankumar, V.S., Madhavan, J., Al-Mayouf, A.M., 2018. An efficient visible light driven bismuth ferrite incorporated bismuth oxyiodide (BiFeO<sub>3</sub>/BiOI) composite photocatalytic material for degradation of pollutants. *Opt. Mater.* 84, 227–235. <https://doi.org/10.1016/j.optmat.2018.06.067>.
- Malato, S., Fernández-Ibáñez, P., Maldonado, M.I., Blanco, J., Gernjak, W., 2009. Decontamination and disinfection of water by solar photocatalysis: recent overview and trends. *Catal. Today* 147 (1), 1–59. <https://doi.org/10.1016/j.cattod.2009.06.018>.
- Man, H.C., Abba, M.U., Abdulsalam, M., Azis, R.S., Idris, A.I., Hamzah, M.H., 2020. Utilization of nano-TiO<sub>2</sub> as an influential additive for complementing separation performance of a hybrid PVDF-PVP hollow fiber: boron removal from Leachate. *Polymers* 12, 2511. <https://doi.org/10.3390/polym12112511>.
- Moslehyani, A., Ismail, A.F., Othman, M.H.D., Matsuura, T., 2015. Design and performance study of hybrid photocatalytic reactor-PVDF/MWCNT nanocomposite membrane system for treatment of petroleum refinery wastewater. *Desalination* 363, 99–111. <https://doi.org/10.1016/j.desal.2015.01.044>.
- Pal, P., 2020. Membrane technology to convert dairy waste into value-added products. *Membrane-Based Technol. Environ. Pollut. Control* 649–701. <https://doi.org/10.1016/b978-0-12-819455-3.00017-0>.
- Pi, X., Zhang, S., Wang, L., Li, H., Hei, Y., Zheng, Z., Luo, L., 2021. BiVO<sub>4</sub> photo-catalyst with controllable wettability and its improved visible light catalytic activity for degradation of 17 $\alpha$ -Ethinylestradiol. *J. Taiwan Inst. Chem. Eng.* 127, 140–150. <https://doi.org/10.1016/j.jtice.2021.07.040>.
- Ratova, M., Redfern, J., Verran, J., Kelly, P.J., 2018. Highly efficient photocatalytic bismuth oxide coatings and their antimicrobial properties under visible light irradiation. *Appl. Catal. B Environ.* 239, 223–232. <https://doi.org/10.1016/j.apcatb.2018.08.020>.
- Riaz, S., Park, S.J., 2019. An overview of TiO<sub>2</sub>-based photocatalytic membrane reactors for water and wastewater treatments. *J. Ind. Eng. Chem.* <https://doi.org/10.1016/j.jiec.2019.12.021>.
- Selvaraj, M., Hai Banat, F., Abu, M., 2020. Application and prospects of carbon nanostructured materials in water treatment: a review. *J. Water Proc. Eng.* 33, 100996 <https://doi.org/10.1016/j.jwpe.2019.100996>. July 20190.
- Srivastava, Harsha P., Arthanareeswaran, G., Anantharaman, N., Starov, Victor M., 2011. Performance of modified poly(vinylidene fluoride) membrane for textile wastewater ultrafiltration. *Desalination* 282, 87–94. <https://doi.org/10.1016/j.desal.2011.05.054>.
- Srivastava, H.P., Arthanareeswaran, G., Anantharaman, N., Starov, V.M., 2011. Performance of modified poly(vinylidene fluoride) membrane for textile wastewater ultrafiltration. *Desalination* 282, 87–94. <https://doi.org/10.1016/j.desal.2011.05.054>.
- Wang, S., Liang, S., Liang, P., Zhang, X., Sun, J., Wu, S., Huang, X., 2015. In-situ combined dual-layer CNT/PVDF membrane for electrically-enhanced fouling resistance. *J. Membr. Sci.* 491, 37–44. <https://doi.org/10.1016/j.memsci.2015.05.014>.
- Yi, Q., Wang, H., Cong, S., Cao, Y., Wang, Y., Sun, Y., Lou, Y., Zhao, J., Wu, J., Zou, G., 2016. Self-cleaning glass of photocatalytic anatase TiO<sub>2</sub>@Carbon nanotubes thin film by PolymerAssisted approach. *I. Nanoscale Res. Lett.* 11, 457. <https://doi.org/10.1186/s11671-016-1674-4>.
- Yogarathinam, L.T., Gangasalam, A., Ismail, A.F., Arumugam, S., Narayanan, A., 2018. Concentration of whey protein from cheese whey effluent using ultrafiltration by combination of hydrophilic metal oxides and hydrophobic polymer. *J. Chem. Technol. Biotechnol.* 93 (9), 2576–2591. <https://doi.org/10.1002/jctb.5611>.
- Zouzelka, R., Kusumawati, Y., Remzova, M., Rathousky, J., Pauporté, T., 2016. Photocatalytic activity of porous multiwalled carbon nanotube-TiO<sub>2</sub> composite layers for pollutant degradation. *J. Hazard Mater.* 317, 52–59. <https://doi.org/10.1016/j.jhazmat.2016.05.056>.
- Nascimben Santos, E., Ágoston, Á., Kertész, S., Hodúr, C., László, Z., Pap, Z., Kása, Z., Alapi, T., Krishnan, S.A.G., Arthanareeswaran, G., 2020. Investigation of the applicability of TiO<sub>2</sub>, BiVO<sub>4</sub>, and WO<sub>3</sub> nanomaterials for advanced photocatalytic membranes used for oil-in-water emulsion separation. *Asia-Pac. J. Chem. Eng.* 15, e2549. <https://doi.org/10.1002/apj.2549>, 2020.